Jinst

Published by IOP Publishing for Sissa Medialab

Received: *December 31, 2023*
Accepted: *February 12, 2024*
Published: *March 27, 2024*

68th ICFA Advanced Beam Dynamics Workshop on High-Intensity and High-Brightness Hadron Beams — HB2023

Impact of beam-coupling impedance on the Schottky spectrum of bunched beam

C. Lannoy[a,b,*] **K. Lasocha**[a] **T. Pieloni**[b] **D. Alves**[a] **and N. Mounet**[a]

[a] *CERN, Geneva, Switzerland*
[b] *Institute of Physics, École polytechnique fédérale de Lausanne (EPFL), CH-1015 Lausanne, Switzerland*

E-mail: christophe.lannoy@cern.ch

Abstract: The Schottky monitors of the Large Hadron Collider (LHC) can be used for non-invasive beam diagnostics to estimate various bunch characteristics, such as tune, chromaticity, bunch profile or synchrotron frequency distribution. However, collective effects, in particular beam-coupling impedance, can significantly affect Schottky spectra when large bunch charges are involved. In such conditions, the available interpretation methods are difficult to apply directly to the measured spectra, thus preventing the extraction of beam and machine parameters, which is possible for lower bunch charges. To study the impact of impedance on such spectra, we introduce a method for building Schottky spectra from macro-particle simulations performed with the PyHEADTAIL code, applied to LHC beam conditions. In this case, the use of a standard Fast Fourier Transform (FFT) algorithm to recover the spectral content of the beam becomes computationally intractable memory-wise, because of the relatively short bunch length compared to the large revolution period. To circumvent this difficulty, a semi-analytical method was developed to efficiently compute the Fourier transform. The simulated Schottky spectrum is then compared against theoretical formulas and measurements of Schottky signals previously obtained with lead ion beams in the LHC where impedance effects are expected to be limited. Furthermore, this study provides preliminary interpretations of the impact of beam-coupling impedance on proton Schottky spectra by incorporating longitudinal and transverse resonator-like impedance models into the simulations. A theoretical framework is also introduced for the case of the longitudinal impedance, allowing the extension of the existing theoretical formalism.

Keywords: Accelerator modelling and simulations (multi-particle dynamics, single-particle dynamics); Instrumentation for particle accelerators and storage rings - high energy (linear accelerators, synchrotrons)

*Corresponding author.

https://doi.org/10.1088/1748-0221/19/03/P03017

2024 JINST 19 P03017

Contents

1 Introduction

Schottky signals contain information on various beam and machine parameters, such as momentum spread, betatron tune, synchrotron frequency and chromaticity, among others. The basic theory of Schottky signals predicts how all of these parameters express themselves in the recorded signal, after it is transformed to the frequency domain. This topic is treated in detail in a classical work by Boussard [1]. The developed theory is however limited to a simple beam dynamics model and does not include, e.g., collective effects and beam interaction with the vacuum chamber through impedance. Due to the complex theoretical description of such effects, it is most suitable to study their impact on Schottky spectra using multi-particle simulations, as done in ref. [2], where the effect of space charge was investigated.

The study presented herein is based on simulations performed with PyHEADTAIL [3, 4], a macro-particle code that can be used to track turn-by-turn the six-dimensional phase space evolution of a bunch, possibly including the effects of direct space charge and beam-coupling impedances. The following section will present the method used to post-process the data from PyHEADTAIL and reconstruct the Schottky spectra. The simulated spectra will be benchmarked against theoretical formalisms and measurements from ion beams in the Large Hadron Collider (LHC) where the effects of beam-coupling impedance are expected to be limited.

In the third section, simulations are performed for the case of LHC proton bunches where impedance effects are present. We explore the impact of longitudinal and transverse impedance on the Schottky spectrum by incorporating longitudinal and transverse resonator-like impedance models in the simulations. Furthermore, the amplitude-dependent synchrotron tune shift arising from longitudinal impedance is discussed theoretically.

2024 JINST 19 P03017

2 Macro-particle simulation method

Obtaining a Schottky spectrum from multi-particle simulations in the case of the LHC, is particularly challenging computationally due to the highly sparse characteristic of the current signal produced by a single bunch. While discretising the current signal in time, and applying the Fast Fourier Transform (FFT) algorithm to retrieve the spectral content of the beam is manageable for smaller accelerators, typically having smaller revolution periods and longer bunches, like the CERN Proton Synchrotron (PS), this is unfortunately intractable memory-wise for the LHC. As a conservative estimate, for the LHC revolution frequency $f_0 \approx 11\,245.5\,\text{Hz}$, if we sample a 1 ns long bunch with 100 points (which corresponds to a sampling frequency of 100 GHz) over 10'000 turns, we would have to store an array of $10^{11+4}/f_0 \sim 10^{11}$ signal samples[1] or around 1 TB of data, hence the need of an alternative approach. In the presented method, the beam's spectral content is calculated concurrently with the macro-particle simulation and stored efficiently, irrespective of the particle count. This approach enables the processing of one million macro-particles in the LHC over 10,000 revolutions within a few hours, using a standard computer.

2.1 Longitudinal spectrum

The longitudinal Schottky spectrum is given by the power spectral density (PSD) of the beam current. The current of a single particle i as seen from a pickup, can be expressed as

$$i_i(t) = q \sum_{n=0}^{N_t} \delta(t - nT_0 - \tau_{n,i}),$$

where δ is the Dirac delta distribution, N_t the number of turns, q the charge of the particle, $f_0 = 1/T_0$ the LHC revolution frequency, and $\tau_{n,i}$ the arrival time difference between the particle i and the synchronous particle at turn n. The current produced by one bunch is simply obtained by summing the contributions of the N_p particles constituting the bunch:

$$i(t) = q \sum_{i=1}^{N_p} \sum_{n=0}^{N_t} \delta(t - nT_0 - \tau_{n,i}).$$

We proceed by computing analytically the Fourier transform

$$\widetilde{i(\omega)} = \int_{-\infty}^{\infty} i(t) e^{j\omega t} dt = q \sum_{n=0}^{N_t} e^{j\omega n T_0} \sum_{i=1}^{N_p} e^{j\omega \tau_{n,i}}. \tag{2.1}$$

To evaluate numerically this last expression we would have to store in memory the $N_t \times N_p$ numbers $\tau_{n,i}$ and to compute $O(N_t N_p N_f)$ exponentials, where N_f is the number of frequencies to be included in the spectrum. Both these requirements are highly limiting the number of particles we can simulate. We expect that the number of macro-particles required to make the PyHEADTAIL simulation realistic would be at least $N_p \sim 10^6$. Typical values for the number of turns and frequencies are $N_t \sim N_f \sim 10^4$ and come respectively from the acquisition time and spectral resolution of the LHC Schottky Monitor.

[1] Most of these will be zeros and while Sparse Fourier Transform algorithms exist, these are only applicable to sparse output signals.

2024 JINST 19 P03017

The spectrum in eq. (2.1) can be computed more efficiently by replacing the right-hand exponential with its Taylor expansion. Since we are interested in the frequency domain of the LHC Schottky monitor working at the $h = 427725$ harmonic of the revolution frequency, the spectrum will only be evaluated for a limited range around the central frequency $\omega_c = 2\pi h f_0$. By respectively defining $\omega = \omega_c + \delta\omega$, replacing the right-most exponential with its Taylor expansion, and inverting the summation order, eq. (2.1) becomes

$$\begin{aligned}
\widetilde{i(\omega)} &= q \sum_{n=0}^{N_t} e^{j\omega n T_0} \sum_{i=1}^{N_p} e^{j\omega_c \tau_{n,i}} e^{j\delta\omega\tau_{n,i}} \\
&= q \sum_{n=0}^{N_t} e^{j\omega n T_0} \sum_{i=1}^{N_p} e^{j\omega_c \tau_{n,i}} \sum_{l=0}^{N_l-1} \frac{(j\delta\omega\tau_{n,i})^l}{l!} + \mathcal{R} \\
&= q \sum_{n=0}^{N_t} e^{j\omega n T_0} \sum_{l=0}^{N_l-1} \frac{(j\delta\omega)^l}{l!} \sum_{i=1}^{N_p} e^{j\omega_c \tau_{n,i}} (\tau_{n,i})^l + \mathcal{R},
\end{aligned}$$

where $\mathcal{R}$ comes from the truncated part of the Taylor expansion. By introducing the variables $\mathcal{L}_{n,l}$ and $\alpha_l(\omega)$ defined as

$$\mathcal{L}_{n,l} = \sum_{i=1}^{N_p} e^{j\omega_c \tau_{n,i}} (\tau_{n,i})^l, \qquad \alpha_l(\omega) = \frac{(j\delta\omega)^l}{l!},$$

and neglecting the rest $\mathcal{R}$, the previous expression can be written in the compact form

$$\widetilde{i(\omega)} = q \sum_{n=0}^{N_t} e^{j\omega n T_0} \sum_{l=0}^{N_l-1} \alpha_l(\omega)\, \mathcal{L}_{n,l}. \tag{2.2}$$

Computing all the $\mathcal{L}$ coefficients requires $O(N_t N_p)$ operations; the summation over N_l can be considered as $O(1)$, hence computing the spectrum thereafter takes $O(N_t N_f)$ operations. The total cost of evaluating eq. (2.2) is then $O(N_t N_p)$ since $N_f \ll N_p$.

The number of terms of the Taylor expansion N_l required to neglect the rest $\mathcal{R}$, can be verified, a posteriori, by checking that the upper bound of $|\mathcal{R}|$ is small enough with respect to the lowest value of interest of $|\widetilde{i(\omega)}|$ computed with eq. (2.2). An upper bound of $|\mathcal{R}|$ can be computed as follows:

$$\begin{aligned}
|\mathcal{R}| &= q \left| \sum_{n=0}^{N_t} e^{j\omega n T_0} \sum_{i=1}^{N_p} e^{j\omega_c \tau_{n,i}} \sum_{l=N_l}^{\infty} \frac{(j\delta\omega\tau_{n,i})^l}{l!} \right| \\
&\leq q N_t N_p \sum_{l=N_l}^{\infty} \frac{|\delta\omega_{\max}\tau_{\max}|^l}{l!} \\
&\leq q N_t N_p \, |\delta\omega_{\max}\tau_{\max}|^{N_l} \sum_{l=0}^{\infty} \frac{|\delta\omega_{\max}\tau_{\max}|^l}{l!} \frac{l!}{(l+N_l)!} \\
&\leq q N_t N_p \frac{|\delta\omega_{\max}\tau_{\max}|^{N_l}}{N_l!} e^{|\delta\omega_{\max}\tau_{\max}|},
\end{aligned} \tag{2.3}$$

where we used the property $\frac{l!}{(l+N_l)!} \leq \frac{1}{N_l!}$ for the last inequality. For typical LHC conditions, $\tau_{\max} \sim 1\,\text{ns}$ and $|\delta\omega_{\max}\tau_{\max}| \sim 10^{-5}$ (considering a longitudinal Schottky spectrum made of ~ 25

2024 JINST 19 P03017

satellites spaced by the nominal synchrotron frequency $f_s \sim 65\,\text{Hz}$). Table 1 presents the relative magnitude of the upper bound of the rest $\mathcal{R}_{\max}$ with respect to the minimal value of interest of the longitudinal spectrum $|\widetilde{i(\omega)}|$ for different value of N_l. For the LHC simulation parameters stated above, $N_l = 3$ or 4 is typically sufficient.[2] As an additional check, the full computation of the Schottky spectrum was also performed with lower values of N_l to verify that convergence was achieved.

2.2 Transverse spectrum

The horizontal and vertical transverse Schottky spectra are given by the PSD of the corresponding dipole moment of the beam. The developments discussed below are carried out for the horizontal plane x but are analogous in every aspect for the vertical plane. With the dipole moment of a single particle i defined as $d_i(t) = x_i(t)\ i_i(t)$, for the full bunch we get:

$$d(t) = q \sum_{i=1}^{N_p} \sum_{n=0}^{N_t} x_{n,i} \delta(t - nT_0 - \tau_{n,i}),$$

where $x_{n,i} = x_i(t = nT_0 + \tau_{n,i}) \approx x_i(t = nT_0)$ is the horizontal transverse position of the particle i when passing in front of the detector at turn n. Following a similar derivation as for the longitudinal spectrum, we compute the Fourier transform of the signal, replace the right-most exponential by its Taylor expansion around ω_c, and invert the summation order, yielding

$$\widetilde{d(\omega)} = \int_{-\infty}^{\infty} d(t) e^{j\omega t} dt = q \sum_{n=0}^{N_t} e^{j\omega n T_0} \sum_{l=0}^{N_l - 1} \frac{(j\delta\omega)^l}{l!} \sum_{i=1}^{N_p} x_{n,i}\ e^{j\omega_c \tau_{n,i}} (\tau_{n,i})^l + \mathcal{R}'.$$

Using the definition

$$\mathcal{T}_{n,l} = \sum_{i=0}^{N_p} x_{n,i}\ e^{j\omega_c \tau_{n,i}} (\tau_{n,i})^l,$$

we get a similar expression as eq. (2.2) where the longitudinal coefficients $\mathcal{L}$ are replaced by the transverse coefficients $\mathcal{T}$

$$\widetilde{d(\omega)} = q \sum_{n=0}^{N_t} e^{j\omega n T_0} \sum_{l=0}^{N_l - 1} \alpha_l(\omega)\ \mathcal{T}_{n,l}. \tag{2.4}$$

Similarly, an upper bound for the rest of the transverse spectrum $\mathcal{R}'$ is given by

$$|\mathcal{R}'| \leq q N_t N_p\ x_{\max} \frac{|\delta\omega_{\max}\tau_{\max}|^{N_l}}{N_l!} e^{|\delta\omega_{\max}\tau_{\max}|},$$

with for the LHC case $x_{\max} \sim 3\,\text{mm}$ and $|\delta\omega_{\max}\tau_{\max}| \sim 3 \times 10^{-5}$ (considering a transverse Schottky sideband made of ~ 25 satellites spaced by the nominal synchrotron frequency $f_s \sim 65\,\text{Hz}$ and for a fractional part of the tune $q_x \sim q_y \sim 0.3$). For these typical LHC simulation parameters, table 1 indicates that $N_l = 3$ or 4 is typically sufficient for the transverse case as well.

Besides the considerable gain in computation time, another advantage of the formalism of eqs. (2.2) and (2.4) is that the $\mathcal{L}$ and $\mathcal{T}$ coefficients can be calculated simultaneously with the tracking done in the PyHEADTAIL simulation. Hence there is no need to keep in memory the extremely large arrays of $\tau_{n,i}$, $x_{n,i}$ and $y_{n,i}$ for each turn and each particle - all the necessary information is contained in the $N_t \times N_l$ coefficients $\mathcal{L}$ and $\mathcal{T}$. Since the number of these coefficients does not depend on the number of macro-particles, we can increase the latter without any concern regarding memory.

[2]The upper bound in eq. (2.3) is actually a large overestimate of the rest and $N_l = 1$ can be sufficient in some cases.

2024 JINST 19 P03017

Table 1. Upper bound relative precision of the simulation for various number of terms in the Taylor expansion.

Number of terms N_l	1	2	3	4
Longitudinal band $\frac{\mathcal{R}_{\max}}{\min\left(\lvert\widetilde{i(\omega)}\rvert\right)}$	1.0×10^{6}	5.0×10^{0}	1.7×10^{-5}	4.2×10^{-11}
Transverse bands $\frac{\mathcal{R}'_{\max}}{\min\left(\lvert\widetilde{d(\omega)}\rvert\right)}$	9.0×10^{6}	1.4×10^{2}	1.4×10^{-3}	1.0×10^{-8}

2.3 Simulation procedure

Figure 1 sketches the full simulation procedure. Note that we use the smooth approximation for the machine optics, and (unless stated otherwise) a non-linear radio frequency (RF) system (hence leading to synchrotron frequency spread).

The spatial coordinates $x_{n,i}$, $y_{n,i}$ and $z_{n,i}$ of each marco-particle at each turn, obtained from PyHEADTAIL, are plugged into eqs. (2.2) and (2.4) to reconstruct the longitudinal and transverse Schottky spectra. Notably, the so-called instantaneous[3] Schottky spectra generated from this simulation procedure will exhibit significant dissimilarities from one simulation to another. This is due to the fact that instantaneous Schottky signals are only a single realisation of a random process, implicitly depending on the discrete distribution of synchrotron and betatron amplitudes and phases among the particles. As described in refs. [6, 7], both the standard deviation and mean value of the PSD are proportional to the number of simulated particles,[4] and therefore increasing the latter will not make the spectrum converge to its true average. To estimate the expected value of the Schottky power spectrum, and reveal the inner structure of the Bessel satellites described by the theory, the averaging of instantaneous Schottky spectra is required, both in simulations and experimental measurements.

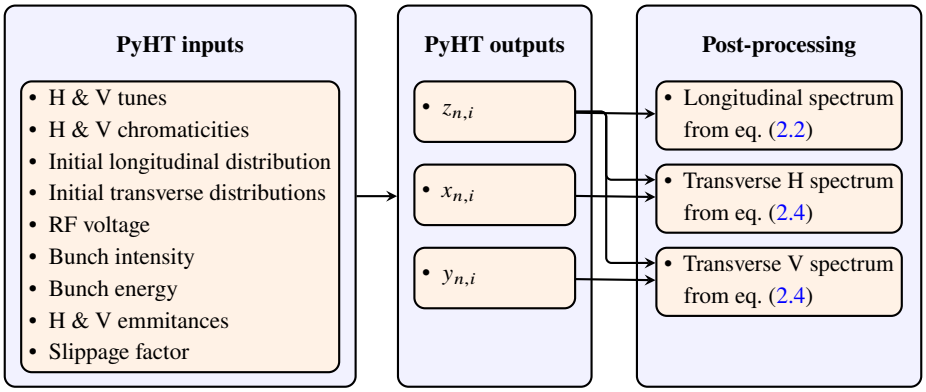

Figure 1. Schottky spectrum simulation procedure.

[3]The term *instantaneous* originates from the measurements where each spectrum is acquired over a given period (~16,000 revolutions). Consecutive measured instantaneous spectra differ significantly due to the drift of the initial betatron and synchrotron phases. This behaviour is analogous in simulations where the initial bunch is a new random draw for each simulation. Therefore, the term *instantaneous* is used to characterise the spectrum produced by a single simulation.

[4]This is not true for the central satellite of the longitudinal band.

2024 JINST 19 P03017

2.4 Experimental benchmarking

The simulation method presented in the previous section is benchmarked against experimental Schottky spectra obtained with lead ion beams during LHC Run 2. The Schottky data consists of horizontal and vertical measurements of beam 2 taken at injection energy during the fill 7443.

Among the PyHEADTAIL input parameters described in figure 1, some are based on the fitting of the experimental spectrum as done in ref. [8, 9] and allow to determine precise machine parameters of the specific fill we want to reproduce. The parameters based on this fitting procedure are horizontal and vertical tunes, horizontal and vertical chromaticities, synchrotron amplitude distribution and nominal synchrotron frequency.[5] The other parameters needed by PyHEADTAIL such as emmitances or bunch intensity and energy, come from direct measurements or machine design. Table 2 summarises the values of these parameters.

Table 2. PyHEADTAIL Simulation Parameters for Fill 7443.

Intensity	1.76×10^8 ions per bunch
Energy per ion	36.9 TeV
Ion charge	$82e$
Ion mass	$193.687\,\mathrm{GeV}/c^2$
ϵ_x, ϵ_y	1.5 µm
Tunes	$Q_x = 64.2827,\ Q_y = 59.2985$
Chromaticities	$Q'_x = 18.56,\ Q'_y = 11.64$
Slippage factor	3.182×10^{-4}
h_{rf}	35640
RF voltage	8.22 MV
LHC circumference	26.659 km
Rice parameters of $\widehat{\tau}$ distribution	$\sigma = 0.216\,\mathrm{ns},\ b = 1.306$

The fitting procedure of ref. [8] assumes that the synchrotron amplitudes $\widehat{\tau}$ follows a Rice distribution and provides the two parameters σ and b of this distribution. On the other hand, the macro-particle simulation requires to have an initial distribution in terms of position z and momentum deviation Δp. The amplitude of the momentum deviation $\widehat{\Delta p}$ can be deduced from $\widehat{\tau}$ by using eqs. (4) and (11) from ref. [10], which yield

$$\widehat{\Delta p} = \frac{p_0}{|\eta|}\widehat{\tau}\left(1 - \frac{(h_{\mathrm{rf}}\omega_0\,\widehat{\tau})^2}{16}\right)\Omega_0\,, \tag{2.5}$$

with p_0 the nominal momentum, η the slippage factor, Ω_0 the nominal angular synchrotron frequency, h_{rf} the radio frequency harmonic and ω_0 the angular revolution frequency of the LHC. The initial position with respect to the synchronous particle z and momentum deviation Δp of each particle can then be computed from their synchrotron amplitude and phase[6] using eqs. (10) and (12) of ref. [10]:

$$z_i = \beta\, c\, \widehat{\tau_i}\ \cos(\phi_i), \qquad \Delta p_i = \widehat{\Delta p_i}\ \sin(\phi_i).$$

[5] Here we define the nominal synchrotron frequency as the limit of the synchrotron frequency for synchrotron amplitudes approaching zero.

[6] Synchrotron phases are assumed to be uniformly distributed.

2024 JINST 19 P03017

The initial transverse positions and momenta are instead obtained assuming a 2D Gaussian distribution in phase space.

Figure 2 presents an overall view of the simulated longitudinal and transverse Schottky spectra obtained using eqs. (2.2) and (2.4) respectively and plotted on the same frequency axis (frequencies in the plot have been shifted from the LHC Schottky harmonic 427725, to the first harmonic of the revolution frequency). Figure 3 is a detailed view of these spectra compared against the experimental measurements of fill 7443. As visible from the plots, the agreement between simulations and measurements is very good. One can also observe that the effect of chromaticity, which makes the upper betatron sideband higher and thinner than the lower sideband, is well reproduced by the simulation.

2.5 Theoretical benchmarking

The simulations are compared against two theory-based methods suitable to reconstruct the Schottky spectrum. The first method is based on the Monte Carlo approach presented in ref. [11]. It consists of drawing randomly, for each particle, a synchrotron oscillation time-amplitude $\widehat{\tau_i}$ and an initial synchrotron phase φ_{s_i} from respectively a Rice and a uniform distribution. Using the theoretical formula for the longitudinal Schottky signal of a given particle i [1]

$$i_i(t) = q f_0 \sum_{n,p=-\infty}^{\infty} J_p(n\omega_0\widehat{\tau_i})\, e^{j(n\omega_0 t + p\Omega_{s_i} t + p\varphi_{s_i})},$$

the Fourier transform of each individual particle can be directly deduced using the expression giving $\Omega_{s_i}(\widehat{\tau_i})$ from ref. [10]. The single particle spectrum exhibits a fine structure characterised by *synchrotron satellites* spaced by the synchrotron frequency Ω_{s_i}. The magnitude of these lines depends on the argument $n\omega_0\widehat{\tau_i}$ and order p of the Bessel function. In general, the synchrotron initial phase φ_{s_i} is responsible for the complex nature of the spectrum. When considering more than one particle in the beam, the synchrotron frequency and phase evolve into random distributions, transforming individual lines into bands. As the Fourier transform is a linear operation, the bunch spectrum can be derived by summing the complex values of single-particle spectra using a sliding window, as done in ref. [11]. Taking the squared modulus of this sum gives the Power Spectral Density (PSD) of the whole bunch (i.e. the Schottky spectrum). Finally, as done for PyHEADTAIL simulations, we need to average the PSD over several random draws for the initial bunch in order to obtain the mean spectrum.

The transverse spectrum is obtained in a similar fashion by drawing an additional initial betatron phase φ_{β_i} from a uniform distribution and using the general expression for the dipole moment from ref. [9]

$$d_i(t) = q f_0 \frac{\widehat{x}}{2} \sum_{n,p=-\infty}^{\infty} J_p(\chi_{i,n}^{\pm}) e^{j(t[(n\pm Q)\omega_0 + p\Omega_{s_i}] \pm \varphi_{\beta_i} + p\varphi_{s_i})},$$

with

$$\chi_{i,n}^{\pm} = (n\eta \pm Q\xi)\, \frac{\omega_0 \widehat{\Delta p_i}}{\Omega_{s_i} p_0},$$

and where Q is the nominal transverse tune, $Q\xi$ the chromaticity, and $\widehat{x}$ the betatron oscillation amplitude. The amplitude of the momentum deviation $\widehat{\Delta p_i}$ is derived from $\widehat{\tau_i}$ with eq. (2.5).

Figure 4 shows a comparison between the results of our proposed simulation-based method, the Monte Carlo method, the matrix formalism developed in refs. [8] and [9], and real measurements

2024 JINST 19 P03017

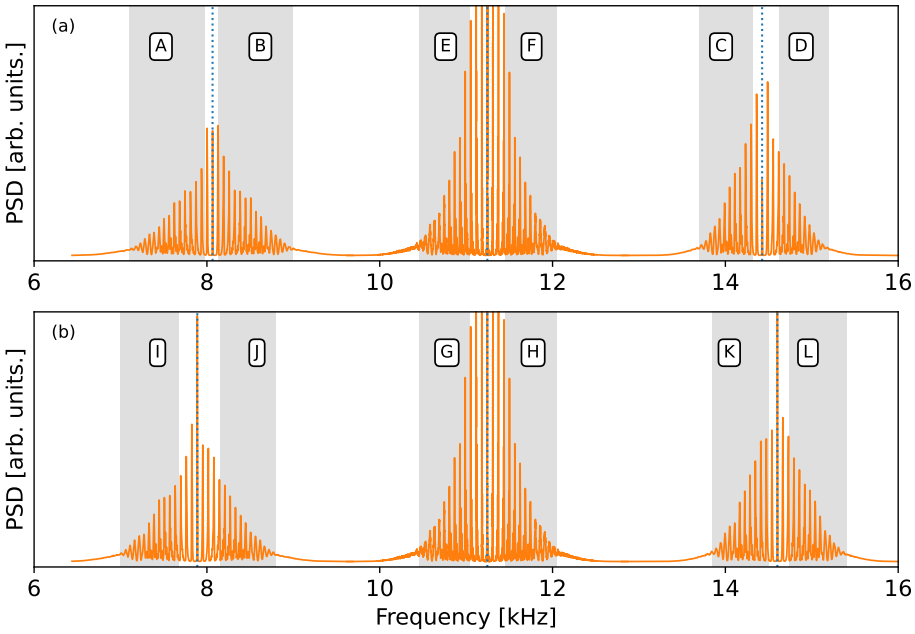

Figure 2. Simulated longitudinal (E, F, G, H), transverse horizontal (A, B, C, D), and transverse vertical (I, J, K, L) Schottky spectra for the machine and beam configuration of LHC fill 7443. The dotted lines indicate respectively (from left to right): $(1 - Q_{x/y})f_0$, f_0 and $(1 + Q_{x/y})f_0$. A detailed view of the shaded region with the corresponding letters is provided in figure 3.

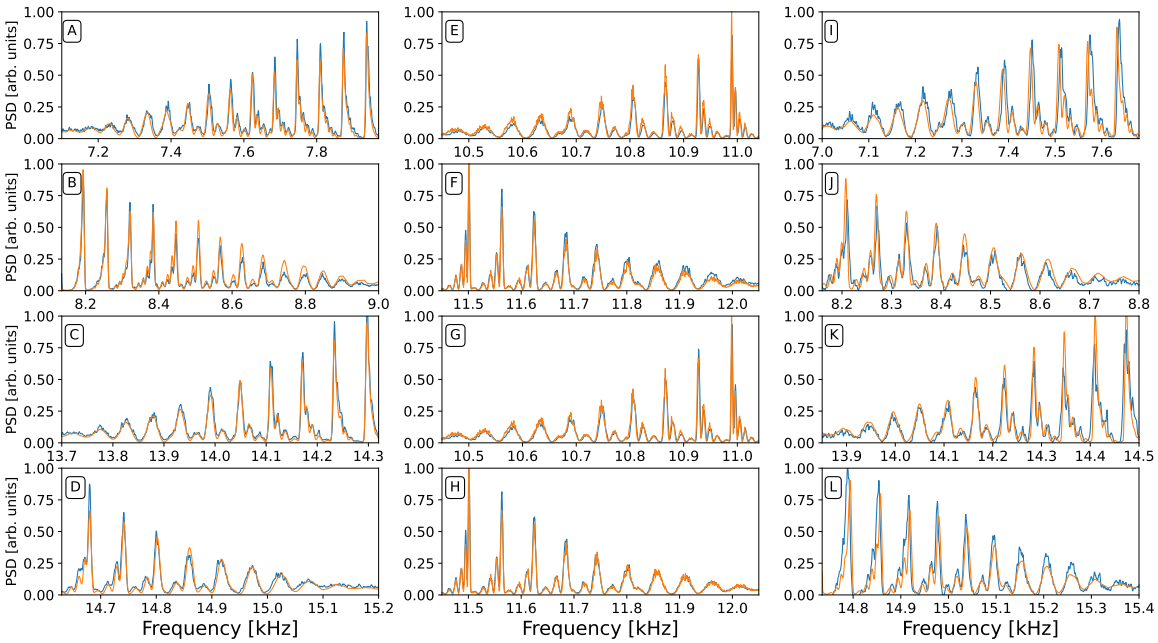

Figure 3. Measured (blue lines) longitudinal and transverse Schottky spectra compared with the simulated spectra (orange lines) for LHC fill 7443. The A–K region labels correspond to the frequency ranges of the shaded regions on figure 2.

2024 JINST 19 P03017

for four different regions of the Schottky spectrum shown in figures 2 and 3. After normalisation, all the spectra are in good agreement with each other.

2.6 Discussion on the simulation methods

While the matrix formalism offers faster computations than macro-particle simulations, this theory is able to describe only relatively simple situations, excluding complex beam dynamics effects such as beam-coupling impedance. Conversely, macro-particle simulations can be more time consuming but provide means to explore the impact of impedance and many other effects.

Besides, the matrix formalism only yields the expected value of Schottky spectra, lacking information on instantaneous spectra or their statistical properties. In contrast, both macro-particle simulations and the Monte-Carlo approach allow the computation of instantaneous spectra, enabling cross-verification of theoretical predictions regarding statistical properties. However, the Monte-Carlo approach, similarly to the matrix formalism, requires an analytical description of the Schottky spectra and is therefore not suitable to study Schottky spectra in the presence of complex collective effects.

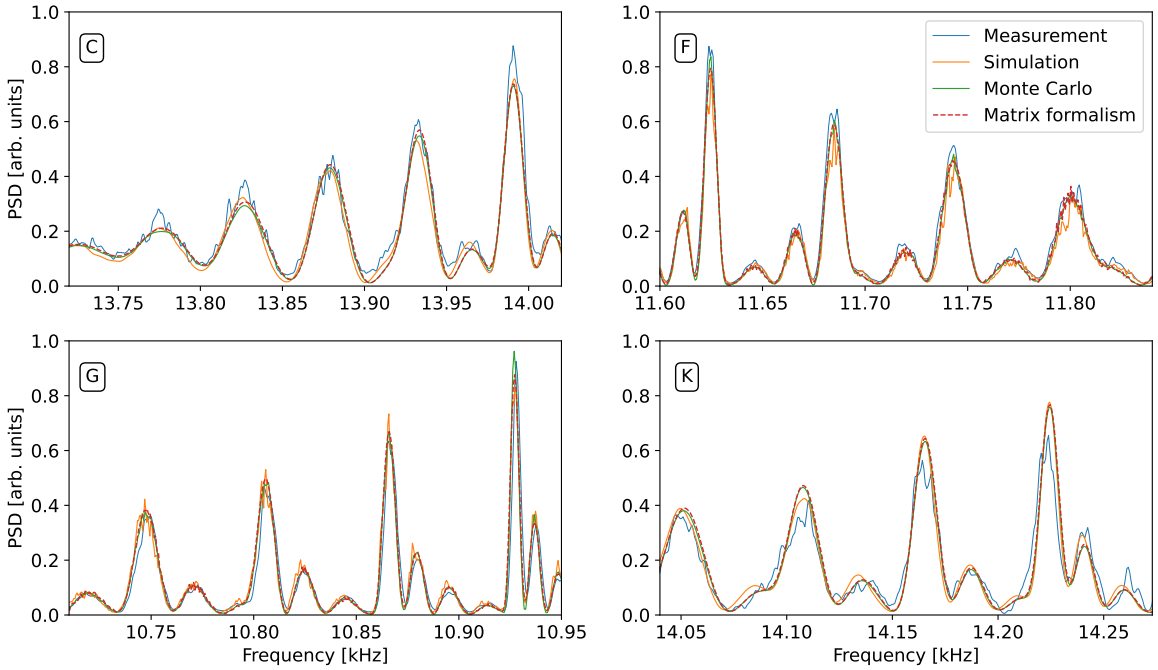

Figure 4. Comparison between measured, simulated, and theoretical, longitudinal (F, G), transverse horizontal (C), and transverse vertical (K) Schottky spectra for LHC fill 7443 (the letters correspond to those defined in Figs 2 and 3).

3 Beam-coupling impedance

In the preceding section, the simulation of an LHC ion bunch was conducted without including any impedance in the PyHEADTAIL simulations. Nevertheless, a good agreement with experimental measurements and existing theories (which also exclude impedance effects) was achieved, showing that the impact of impedance is negligible for LHC ion bunches at injection energy, which could have been anticipated as the bunch charge is relatively low.

2024 JINST 19 P03017

However, for high-intensity LHC proton bunches, a quantitative and accurate interpretation of Schottky spectra can become more challenging due to the increased influence of beam-coupling impedance. Existing theoretical frameworks for Schottky spectrum reconstruction [1, 8, 9, 11] do not account for impedance effects. This section investigates, both theoretically and through simulations, how the spectra are influenced by impedance, starting with the longitudinal case and subsequently exploring the transverse case.

3.1 Longitudinal impedance

Theoretical reconstructions of Schottky spectra, such as the matrix formalism or the Monte Carlo approach mentioned above, are based on the assumption that the synchrotron frequency distribution is known. Under certain conditions, one can derive an analytical relation between the amplitude of the synchrotron oscillation and its frequency (see below) allowing these methods to reconstruct the Schottky spectrum from the synchrotron amplitude distribution. However, this relation has to be modified when additional forces, such as the one coming from beam-coupling impedance, affect the longitudinal dynamics.

This section will briefly present the available theory relating the amplitude of the synchrotron oscillation to its frequency, as well as a commonly adopted approximation. Subsequently, we will deal with the additional forces coming from impedance, extending the theory presented in ref. [12] to the case of a non-linear RF bucket. The developed theory will be applied to the particular case of a longitudinal broad-band resonator, and benchmarked against macro-particle simulations.

3.1.1 Theoretical description

Synchrotron oscillation. For an impedance-free environment, the equation of motion for the RF phase ϕ[7] of a given particle is (eq. (9.51) of ref. [13]):

$$\frac{d^2\phi}{dt^2} + \Omega_0^2 \sin\phi = 0, \tag{3.1}$$

assuming that the synchronous phase ϕ_s is such that $\sin\phi_s$ is small enough to be neglected (i.e. no acceleration or energy loss compensation). The nominal synchrotron frequency reads

$$\Omega_0^2 = \omega_0^2 \frac{-\eta h_{\mathrm{rf}} e\widehat{V}}{2\pi E_0 \beta^2} \cos\phi_s, \tag{3.2}$$

where e is the elementary charge, and where the relevant machine parameters are: the revolution frequency ω_0, the slippage factor η, the amplitude of the RF voltage $\widehat{V}$, the RF harmonic number h_{rf}, the relativistic factor β, and the reference energy E_0. Note that by convention η is positive above transition, such that η and $\cos\phi_s$ always have opposite sign.

Equation (3.1) is identical to the non-linear pendulum equation studied in [14], hence the synchrotron frequency Ω_s of the particle can be written

$$\Omega_s(\widehat{\phi}) = \frac{\pi}{2\mathcal{K}\left[\sin\left(\frac{\widehat{\phi}}{2}\right)\right]}\Omega_0, \tag{3.3}$$

[7]Above transition ϕ has to be taken as the difference between the RF phase of the particle and π.

2024 JINST 19 P03017

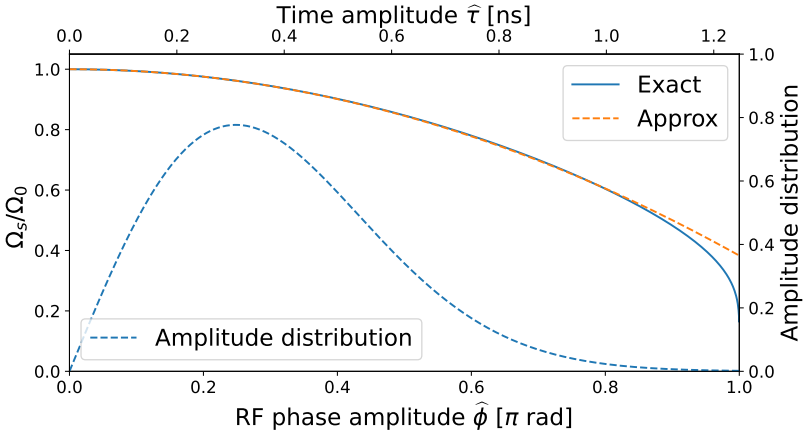

Figure 5. Comparison between the exact (eq. (3.3)) and approximate (eq. (3.5)) expressions of the synchrotron frequency as a function of the oscillation amplitude. The distribution of amplitudes for a Gaussian bunch of RMS $\sigma = 0.31$ ns is also shown.

where $\widehat{\phi}$ is the RF phase amplitude of the synchrotron oscillation and $\mathcal{K}$ is the complete elliptic integral of the first kind given by eq. (8.112.1) of ref. [15].

Equation (3.1) can also be approximated by replacing the sine function with its Maclaurin series expansion up to the third order, which yields

$$\frac{d^2\phi}{dt^2} + \Omega_0^2 \left(\phi - \frac{\phi^3}{6}\right) + O(\phi^5) = 0. \tag{3.4}$$

This last equation has been studied in [14], and an approximation of the oscillation frequency is given by

$$\Omega_s(\widehat{\phi}) = \Omega_0 \left(1 - \frac{\widehat{\phi}^2}{16}\right). \tag{3.5}$$

Figure 5 illustrates how the exact solution from eq. (3.3) compares with the approximation from eq. (3.5). The amplitude distribution corresponding to a Gaussian bunch profile of standard deviation $\sigma = 0.31$ ns is also shown in order to compare the most populated region with the range where the approximation is valid. As can be seen, the approximation holds for an amplitude $\widehat{\phi} \lesssim 0.8\pi$, which is the region where the vast majority of the particles are. Noting that since $\phi = h_{\mathrm{rf}}\omega_0\tau$, with τ the arrival time difference between a given particle and the synchronous particle, we can also express the amplitude of the synchrotron oscillation in terms of the time amplitude given by

$$\widehat{\tau} = \widehat{\phi}/h_{\mathrm{rf}}\omega_0. \tag{3.6}$$

Impedance effect on the longitudinal dynamics. In this section, we investigate the influence of impedance on the longitudinal dynamics of a particle and, more specifically, how it can affect its oscillation frequency. A given force F_i acting longitudinally on the particle will impact the phase dynamics with

$$F_i = \frac{dp}{dt} = \frac{d(p_0 + \delta p)}{dt} = \frac{d(\delta p)}{dt} = \frac{p_0}{\eta}\ddot{\tau} = \frac{p_0}{\eta h_{\mathrm{rf}}\omega_0}\ddot{\phi}, \tag{3.7}$$

2024 JINST 19 P03017

where we used the fact that p_0 is constant, the definition of the slippage factor, and eq. (3.6). The equation of motion with an additional external force is given by combining eqs. (3.1) and (3.7), which yields

$$\ddot{\phi} + \Omega_0^2 \sin\phi = \frac{\eta h \omega_0}{p_0} F_i(t). \tag{3.8}$$

In this study, we focus on the force arising from the longitudinal beam-coupling impedance, which is given by eq. (4.18) of ref. [16]

$$\begin{aligned} F_{\mathrm{Imp}}(t) &= e\left[\vec{E} + \vec{\beta} c \times \vec{B}\right]_{\parallel}\left(t, z = \beta c \tau(t)\right) \\ &= -\frac{Ne^2}{2\pi C}\int_{-\infty}^{\infty} Z_{\parallel}(\omega)\widehat{\Lambda}(\omega) e^{j\frac{\omega z}{\beta c}} d\omega, \end{aligned} \tag{3.9}$$

where C stands for the circumference of the accelerator, N for the number of particles in the bunch, $Z_{\parallel}(\omega)$ for the longitudinal impedance, and $\widehat{\Lambda}(\omega)$ for the beam spectrum normalised by the bunch intensity. The force has to be taken at the current position of the particle, i.e. at a distance $z = \beta c \tau$ behind the synchronous particle. Note that the bunch spectrum $\widehat{\lambda}(\omega)$ in eq. (4.18) of ref. [16], has been replaced by the beam spectrum $\widehat{\Lambda}(\omega)$ in order to take into account the possible multi-turn wake (this approach is equivalent to adding the forces coming from different turns).

The beam spectrum is the Fourier transform of the beam profile. For a single bunch in a circular accelerator, the latter can be expressed as the convolution of the bunch profile $\lambda(t)$ with a Dirac comb of the revolution period T_0. Using the convolution theorem, the beam spectrum can be written

$$\begin{aligned} \widehat{\Lambda}(\omega) &= \mathcal{F}\left\{\lambda(t) * \text{Ш}_{T_0}(t)\right\} \\ &= \mathcal{F}\left\{\lambda(t)\right\} \mathcal{F}\left\{\text{Ш}_{T_0}(t)\right\} \\ &= \widehat{\lambda}(\omega)\omega_0 \text{Ш}_{\omega_0}(\omega), \end{aligned} \tag{3.10}$$

where $*$ stands for the convolution operation and where the Dirac comb of period T_0 is defined as follows

$$\text{Ш}_{T_0}(t) = \sum_{p=-\infty}^{\infty} \delta(t - pT_0).$$

Substituting eq. (3.10) in eq. (3.9) , we have

$$\begin{aligned} F_{Imp}(t) &= \frac{-Ie}{C}\sum_{p=-\infty}^{\infty}\int_{-\infty}^{\infty} Z_{\parallel}(\omega)\widehat{\lambda}(\omega) e^{j\frac{\omega z}{\beta c}}\delta(\omega - p\omega_0) d\omega \\ &= \frac{-Ie}{C}\sum_{p=-\infty}^{\infty} Z_{\parallel}(p)\widehat{\lambda}(p) e^{jp\omega_0\tau(t)}, \end{aligned} \tag{3.11}$$

where we used the compact notation $Z_{\parallel}(p) \equiv Z_{\parallel}(p\omega_0)$, $\widehat{\lambda}(p) \equiv \widehat{\lambda}(p\omega_0)$, and the average current $I \equiv Ne\frac{\omega_0}{2\pi}$.

Combining eqs. (3.2), (3.6), (3.8), and (3.11) yields

$$\ddot{\phi} + \Omega_0^2 \sin\phi = \Omega_0^2 \frac{I}{\widehat{V}\cos\phi_s}\sum_{p=-\infty}^{\infty} Z_{\parallel}(p)\widehat{\lambda}(p) e^{j\frac{p}{h_{\mathrm{rf}}}\phi}. \tag{3.12}$$

2024 JINST 19 P03017

By expanding the sine and exponential functions into their Maclaurin series

$$\sin\phi = \sum_{n=0}^{\infty} \frac{(-1)^n}{(2n+1)!}\phi^{2n+1}, \qquad e^{j\frac{p}{h_{\rm rf}}\phi} = \sum_{n=0}^{\infty} \frac{1}{n!}\left(\frac{jp}{h_{\rm rf}}\right)^n \phi^n,$$

eq. (3.12) can be written in the compact form

$$\ddot{\phi} + \Omega_0^2 \sum_{n=0}^{\infty} S_n \phi^n = 0, \tag{3.13}$$

with the coefficients S_n defined by

$$S_n = \begin{cases} -Z_n & : n \text{ even}, \\ \frac{j^{n-1}}{n!} - Z_n & : n \text{ odd}, \end{cases} \tag{3.14}$$

and

$$\begin{aligned} Z_n &= \frac{I}{\widehat{V}\cos\phi_s} \sum_{p=-\infty}^{\infty} Z_\parallel(p)\widehat{\lambda}(p)\frac{1}{n!}\left(\frac{jp}{h}\right)^n \\ &= \frac{Ij^n}{\widehat{V}\cos\phi_s\, n! h_{\rm rf}^n} \sum_{p=-\infty}^{\infty} \widehat{\lambda}(p)p^n \times \begin{cases} Re[Z_\parallel(p)] & : n \text{ even}, \\ j\, Im[Z_\parallel(p)] & : n \text{ odd}. \end{cases} \end{aligned}$$

In the last equality, we used the fact that $\widehat{\lambda}(p)$, $Re\left[Z_\parallel(p)\right]$, and $Im\left[Z_\parallel(p)\right]$ are respectively even, even, and odd functions.

The expansion performed above is motivated by the assumption that for small oscillation amplitudes, only the first-order term plays a significant role. In this context, the shift of the nominal synchrotron frequency is determined by the term represented by S_1. On the other hand, the higher-order, non-linear terms contribute to an amplitude-dependent synchrotron frequency shift.

Note that in a fully self-consistent picture, the forces arising from impedance would actually modify the bunch profile, hence influencing the impedance force in return. The analysis in this section proceeds under the assumption that the modification of the bunch profile due to impedance is sufficiently negligible, allowing the impedance force to be defined from the original Gaussian longitudinal bunch profile.

Broad-band resonator. We will now apply eq. (3.13) to the particular case of a broad-band resonator described by the following function

$$Z_\parallel^{BB}(\omega) = \frac{R_\parallel}{1 - jQ\left(\frac{\omega_r}{\omega} - \frac{\omega}{\omega_r}\right)},$$

where $R_\parallel$ is the shunt impedance, ω_r the angular cut-off frequency, and Q the quality factor. The values we will use for these parameters are shown in table 3.

The even terms in eq. (3.13) are responsible for the synchronous phase shift and, in the particular case of a broad-band resonator, their contribution can be neglected (see appendix A). Expanding eq. (3.13) up to the third order gives

$$\ddot{\phi} + \Omega_0^2\left(S_1\phi + S_3\phi^3\right) + O(\phi^5) = 0, \tag{3.15}$$

2024 JINST 19 P03017

which is similar to eq. (3.4) where the factors 1 and $-\frac{1}{6}$ have been generalised to the arbitrary coefficients S_1 and S_3.

Substituting $\phi_1(t) = \sqrt{A}\phi_2(t)$ in eq. (3.4) yields

$$\ddot{\phi}_2 + \Omega_0^2(\phi_2 - \frac{A}{6}\phi_2^3) = 0, \tag{3.16}$$

and since the two functions $\phi_1(t)$ and $\phi_2(t)$ only differ by a constant factor $\sqrt{A}$, they have the same oscillation frequency and $\widehat{\phi_1} = \sqrt{A}\ \widehat{\phi_2}$:

$$\Omega_{s,\phi_1}(\widehat{\phi_1}) = \Omega_0(1 - \frac{\widehat{\phi_1^2}}{16}) = \Omega_0(1 - \frac{A\ \widehat{\phi_2^2}}{16}) = \Omega_{s,\phi_2}(\widehat{\phi_2}).$$

By defining $\Omega_0' = \Omega_0\sqrt{S_1}$ and $\frac{S_3}{S_1} = \frac{-A}{6}$, eq. (3.15) is identical to eq. (3.16) and the synchrotron frequency in presence of impedance is given by:

$$\Omega_s(\widehat{\phi}) = \Omega_0'(1 - \frac{A\ \widehat{\phi^2}}{16}) = \Omega_0\sqrt{S_1}\left(1 + \frac{3S_3}{8S_1}\widehat{\phi^2}\right). \tag{3.17}$$

This last equation can be used to extend the theoretical matrix formalism introduced in refs. [8, 9] to include longitudinal impedance effects. The original relation between synchrotron amplitudes and frequencies given by eq. (3.5) is replaced by eq. (3.17) to take into account the effect of impedance.

3.1.2 Macro-particle simulations

PyHEADTAIL simulations of an LHC proton bunch at injection energy have been performed following the simulation method presented above. The relevant simulation parameters are given in table 3 and different longitudinal broad-band resonators of varying shunt impedance $R_\parallel$ have been included in the simulations.

Table 3. PyHEADTAIL simulation parameters.

Intensity	1.5×10^{11} protons per bunch
Energy per proton	450 GeV
Emittances	$\epsilon_x = \epsilon_y = 2\,\mu$m
Tunes	$Q_x = 64.28$, $Q_y = 59.29$
Chromaticities	$Q'_x = Q'_y = 0$
Slippage factor	3.436×10^{-4}
RF harmonic	35640
RF voltage	4 MV
LHC circumference	26.659 km
Bunch length (RMS of Gaussian profile)	$\sigma = 0.31$ ns
Longitudinal broad-band resonator	
Shunt impedance	$R_\parallel = 30\,$kΩ or 60 kΩ
Cut-off frequency	$\omega_r = 2\pi \times 5$ GHz
Quality factor	$Q = 1$

Figure 6 presents an overall view of the simulated longitudinal and transverse Schottky spectra together with a detailed view of some regions. The spectra calculated with the matrix formalism

2024 JINST 19 P03017

including impedance effects are also shown for comparison. It can be observed that the broad-band resonator induces a shift of the nominal synchrotron frequency (all satellites moving toward the central one within each band). This shift is due to the term S_1 and the new nominal synchrotron frequency is $\Omega_0\sqrt{S_1}$. The broad-band resonator will reduce the nominal synchrotron frequency for a machine operating above transition, as can be seen from eq. (3.14) (the opposite happens below transition). One can also observe in figure 6 an amplitude-dependent synchrotron frequency shift, as the alterations in the satellite shapes can not be explained by a simple linear transformation involving shifting and scaling of the original form. This effect is due to the higher order terms $S_{2n+1},\ n \geq 1$ in eq. (3.13).

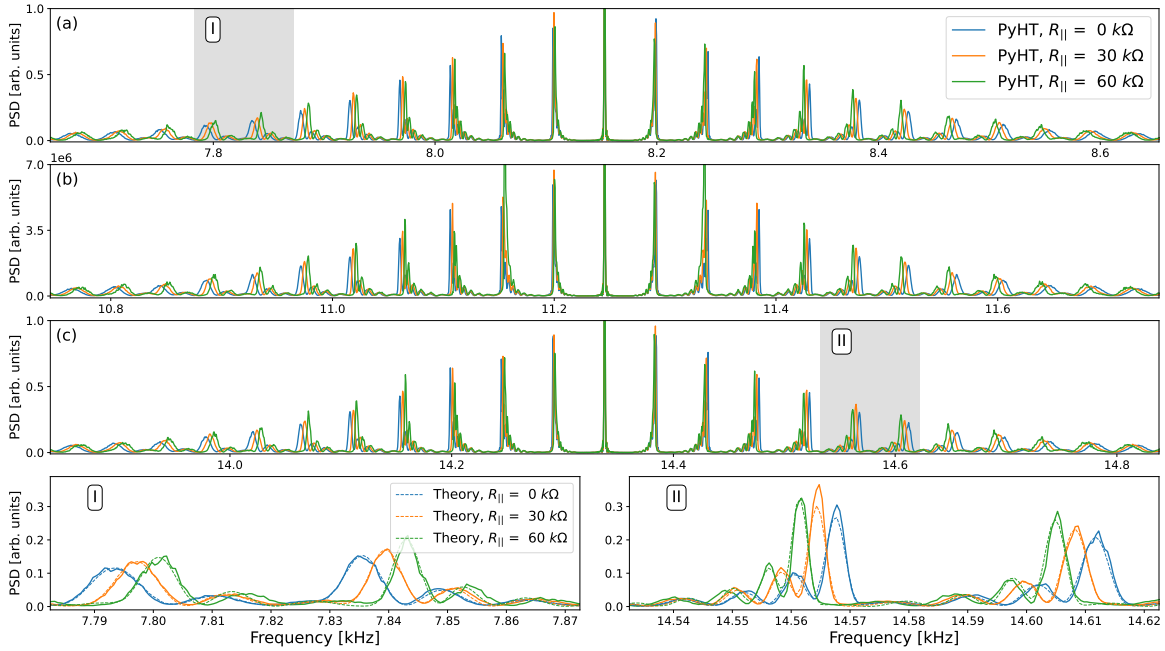

Figure 6. Simulated longitudinal (b) and transverse (a,c) Schottky spectra impacted by a longitudinal broad-band resonator for various shunt impedance. The dashed lines in the two lower plots are obtained from the matrix formalism.

To highlight the amplitude-dependent effects of the synchrotron tune shift, figure 7 illustrates spectra calculated using the matrix formalism, retaining either the first-order or both the first and third-order terms in eq. (3.17). The dotted grey line corresponds to the matrix formalism where only the first order term of the impedance contribution has been kept (i.e. $Z_1 \neq 0$ and $Z_3 = 0$, which corresponds to $S_1 = 1 - Z_1$ and $S_3 = -1/6$ in eq. (3.17)). As can be seen, the nominal synchrotron frequency shift is well reproduced by the theory, while the shift for non-zero amplitude particles, requires higher order terms. The dashed orange line also includes the third order term of the impedance contribution (i.e. $Z_1 \neq 0$ and $Z_3 \neq 0$, which corresponds to $S_1 = 1 - Z_1$ and $S_3 = -1/6 - Z_3$). With the third order impedance term, the theory is in good agreement with the simulation.

One can also probe the validity of eq. (3.17) by directly extracting the relation $\Omega_s(\widehat{\phi})$ from the macro-particle simulation. This was done in figure 8 where each black dot corresponds to the synchrotron amplitude and frequency of a given macro-particle. As before, one can observe that the nominal synchrotron frequency shift is well reproduced by the first order term Z_1, while the shift for larger amplitude particles is correct with the third order theory, up to a certain amplitude $\widehat{\phi} \sim 1.25$ rad.

2024 JINST 19 P03017

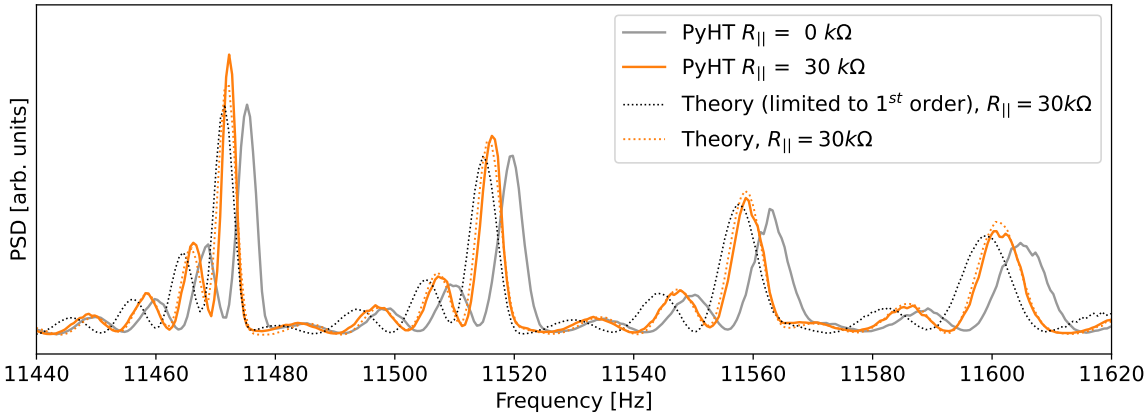

Figure 7. Comparison of the longitudinal Schottky spectrum from the macro-particle simulation against the adapted matrix formalism, with eq. (3.17) including impedance terms Z_n up to the first and third order.

In order to extend the region where eq. (3.17) is valid, one would need to take into account the fifth order term S_5, in the equation of motion. However, this is not crucial since the majority of the particles are well described, as can be seen from the amplitude distribution.

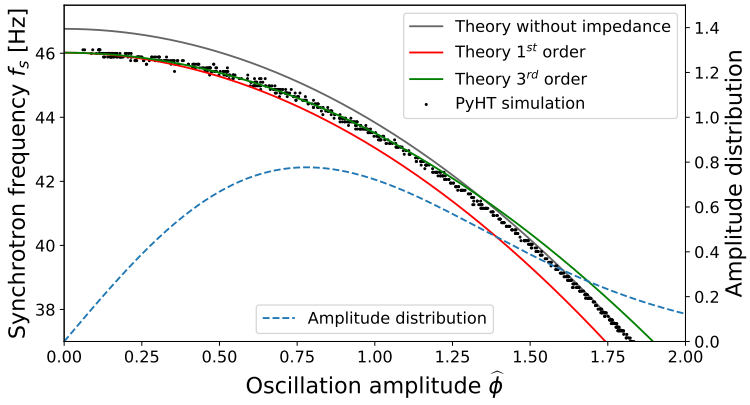

Figure 8. Comparison of eq. (3.17) including impedance terms Z_n up to the first (red) and third (green) order, against macro-particle simulation (black dots). The simulation has been conducted with a longitudinal BB resonator of shunt impedance $R_{||} = 30\,\mathrm{k}\Omega$.

3.2 Transverse impedance

In this last section, a preliminary study on the effects of transverse impedance is conducted through simulations for an LHC proton bunch. The simulation parameters are identical to the one presented in table 3, but the longitudinal broad-band resonator is replaced by a transverse one whose parameters are given in table 4. The transverse broad-band resonator is placed in the horizontal plane and is defined by the following impedance function:

$$Z_{\perp}^{BB}(\omega) = \frac{\omega_r}{\omega} \frac{R_{\perp}}{1 - jQ\left(\frac{\omega_r}{\omega} - \frac{\omega}{\omega_r}\right)}.$$

2024 JINST 19 P03017

Table 4. Transverse broad-band resonator.

Shunt impedance	$R_\perp = 2\,\mathrm{M\Omega\,m^{-1}}$ or $4\,\mathrm{M\Omega\,m^{-1}}$
Cut-off frequency	$\omega_r = 2\pi \times 5\,\mathrm{GHz}$
Quality factor	$Q = 1$

It is worth noting that only the quadrupolar part of the impedance affects the Schottky spectrum. Indeed, as the dipolar wake is proportional to the transverse offset of the leading particle, the total dipolar wake of the bunch cancels out for a stable beam where the bunch is symmetrically centered on the design orbit. The situation is different for the quadrupolar wake, which is proportional to the offset of the trailing particle and does not depend on the leading particle's position.

The effects on the Schottky spectrum can be observed in figure 9. The longitudinal band is not affected by the transverse impedance, while a betatron tune shift is visible on the transverse bands (all satellites in a given transverse sideband are displaced in the same direction). The direction of the satellite's shift - toward the right (resp. left) for the lower (resp. upper) sideband – indicates that the broad-band resonator decreases the betatron tune. Similarly to the case of the longitudinal impedance, the satellites are not simply shifted but their internal structure is also affected by impedance.

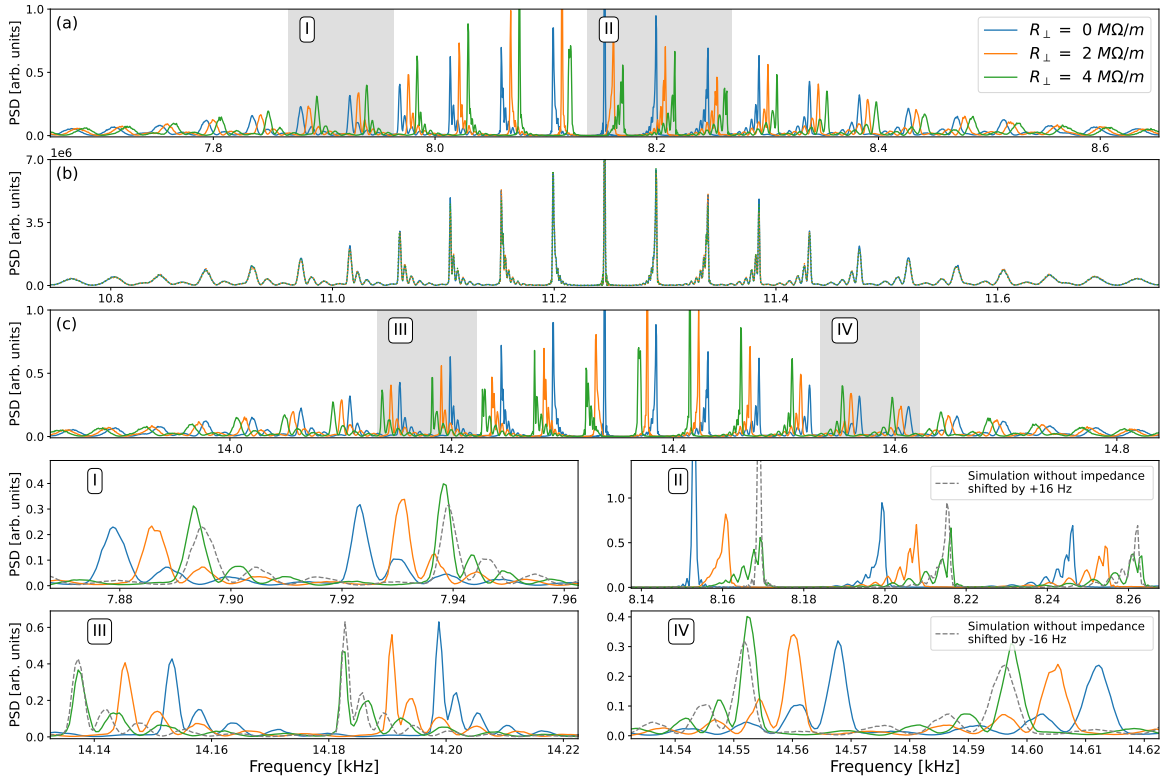

Figure 9. Simulated longitudinal (b), and horizontal (a — lower sideband — and c — upper sideband) Schottky spectra without (blue) and with (orange and green) a transverse BB resonator. Frequencies are shifted from the LHC Schottky harmonic 427725, to the 1st harmonic.

2024 JINST 19 P03017

4 Conclusion

We proposed a new method for computing Schottky spectra from macro-particle simulations, facilitating future investigations into the impact of collective effects, such as beam-coupling impedances, on measured spectra. After discussing the high computational resource requirements of traditional FFT algorithms when performing simulations for LHC beam and machine conditions, we showed how one can achieve a substantial reduction of its computational complexity. The obtained results were shown to be in good agreement with reference measurements as well as with other theory-based methods, and reproduce the overall shape of the spectrum together with the detailed internal structure of the synchrotron satellites, thus validating the method.

Going one step further, we then explored the influence of longitudinal and transverse impedance on the Schottky spectrum, presenting a generalised theory applicable to any kind of longitudinal impedance, and demonstrating agreement with simulations. The findings reveal that longitudinal impedance can induce amplitude-dependent shifts in the synchrotron frequency while the presence of a transverse impedance leads to betatron tune shifts. Both longitudinal and transverse impedance also alter the internal structure of transverse satellites, as shown on various examples using broadband resonators, and also confirmed by the theory presented in the longitudinal case.

Acknowledgments

This article is an updated version of the HB 2023 conference proceeding, published under CC BY 3.0 license as [5].

A Approximation of the longitudinal equation of motion

In order to derive an analytical relation between the amplitude of the synchrotron oscillation and its frequency, we assumed that the even terms in eq. (3.13) can be neglected. In the following, we present how one can assess if this approximation is valid for a given impedance $Z_\parallel(p)$.

The complex exponential in eq. (3.12) can also be expanded with the trigonometric functions

$$\ddot{\phi} + \Omega_0^2 \sin\phi = \frac{\Omega_0^2\, I}{\widehat{V}\cos\phi_s} \sum_{p=-\infty}^{\infty} Z_\parallel(p)\widehat{\lambda}(p) \left(\cos\left(\frac{p}{h_{\mathrm{rf}}}\phi\right) + j\sin\left(\frac{p}{h_{\mathrm{rf}}}\phi\right)\right). \tag{A.1}$$

The cosine term is an even function and corresponds to the sum of all the even terms from eq. (3.13).

A first approximation of the RF phase shift for a particle of given synchrotron time-amplitude $\widehat{\tau}$ is given by the time average of the sum of the even terms:

$$\Delta\phi_s(\widehat{\tau}) = \frac{I}{S_1\widehat{V}\cos\phi_s} \sum_{p=-\infty}^{\infty} Re\big[Z_\parallel(p)\big]\, \widehat{\lambda}(p) \left\langle \cos\left(\frac{p}{h_{\mathrm{rf}}}\phi(t)\right)\right\rangle_t, \tag{A.2}$$

where $\langle\,\rangle_t$ denotes the average value over time. In the limit of small amplitude oscillations, eq. (A.2) reduces to the linear theory, leading to eq. (59) in ref. [12]. By approximating the longitudinal motion of the particle with a harmonic motion [1, 8], we can write

$$\phi(t) = h_{\mathrm{rf}}\omega_0\widehat{\tau}\sin(\Omega_s t + \varphi_s),$$

2024 JINST 19 P03017

with φ_s, the initial phase of the synchrotron oscillation. The average value of the time-dependent part of eq. (A.2) becomes

$$\left\langle \cos\left(\frac{p}{h_{\mathrm{rf}}}\phi(t)\right)\right\rangle_t = \frac{1}{2\pi}\int_0^{2\pi} \cos\left(p\omega_0\widehat{\tau}\sin(t)\right)dt$$
$$= J_0(p\omega_0\widehat{\tau}),$$

using eq. (3.715.10) from [15] for the integral and with J_0, the zero order Bessel function of the first kind.

The average RF phase shift is given by the weighted average of the single particle phase shift

$$\Delta\phi_s = \int_0^{\infty} \Delta\phi_s(\widehat{\tau})g(\widehat{\tau})d\widehat{\tau}$$
$$= \frac{I}{S_1\widehat{V}\cos\phi_s}\sum_{p=-\infty}^{\infty} Re\left[Z_{\parallel}(p)\right]\widehat{\lambda}(p)\int_0^{\infty} J_0(p\omega_0\widehat{\tau})g(\widehat{\tau})d\widehat{\tau},$$

where $g(\widehat{\tau})$ is the distribution of synchrotron oscillation amplitudes. Using the Fourier-Hankel-Abel cycle, it can be shown that the last integral corresponds to the bunch spectrum $\widehat{\lambda}(p)$, which yields

$$\Delta\phi_s = \frac{I}{S_1\widehat{V}\cos\phi_s}\sum_{p=-\infty}^{\infty} Re\left[Z_{\parallel}(p)\right]\widehat{\lambda}^2(p), \tag{A.3}$$

and the total energy lost during one revolution is given by

$$\Delta E_{\mathrm{bunch}} = -Ne\widehat{V}\cos\phi_s S_1\Delta\phi_s$$
$$= -\frac{Q^2}{2\pi}\omega_0\sum_{p=-\infty}^{\infty} Re\left[Z_{\parallel}(p)\right]\widehat{\lambda}^2(p), \tag{A.4}$$

where $Q = Ne$ is the total charge of the bunch. The S_1 factor in eq. (A.4) accounts for the first order potential well distortion due to impedance. This expression is consistent with other formulas available in the literature, such as eq. (4.35) in [16].

In the case of the broad-band resonator defined in table 3 with $R_{\parallel} = 60\,\mathrm{k\Omega}$, we have $\Delta\phi_s = -1.87\,\mathrm{mrad}$ with eq. (A.3), in relative agreement with $\Delta\phi_s = -2.14\,\mathrm{mrad}$ from the macro-particle simulation as shown in figure 10. Such a phase shift is small enough to be neglected, hence we can drop the even terms in eq. (3.13).

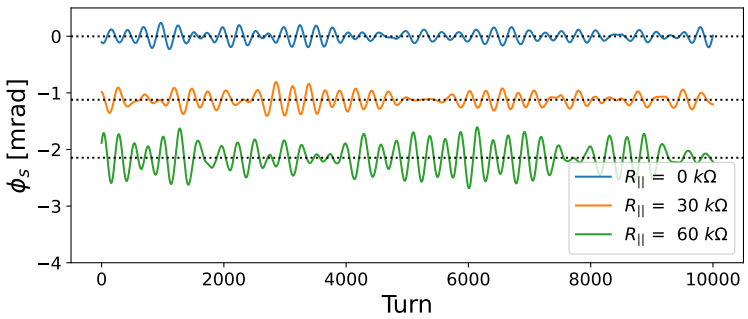

Figure 10. Synchronous phase shift from simulation.

References

[1] D. Boussard, *Schottky noise and beam transfer function diagnostics*, in *CERN Accelerator School: Advanced Accelerator Physics*, CERN-SPS-86-11-ARF (1986) [DOI:10.5170/CERN-1987-003-V-2.416].

[2] O. Boine-Frankenheim and V. Kornilov, *Transverse Schottky noise spectrum for bunches with space charge*, *Phys. Rev. ST Accel. Beams* **12** (2009) 114201.

[3] K. Li et al., *Code development for collective effects*, in the proceedings of the *57th ICFA Advanced Beam Dynamics Workshop on High-Intensity and High-Brightness Hadron Beams*, Malmö, Sweden, 3–8 July 2016 [DOI:10.18429/JACoW-HB2016-WEAM3X01].

[4] PyHEADTAIL code repository, https://github.com/PyCOMPLETE.

[5] C. Lannoy, D. alves, K. Lasocha, N. Mounet, T. Pieloni, *Studies on the Effect of Beam-Coupling Impedance on Schottky Spectra of Bunched Beams* in the proceedings of the *68*th *ICFA Advanced Beam Dynamics Workshop on High-Intensity and High-Brightness Hadron Beams — HB2023*, Geneva, Switzerland, 9–13 October 2023, https://hb2023.vrws.de/papers/thbp47.pdf

[6] C. Lannoy et al., *Statistical Properties of Schottky Spectra*, *JACoW* **IBIC2023** (2023) WEP035.

[7] C. Lannoy, *Statistical properties of Schottky spectra*, CERN note, in preparation.

[8] K. Lasocha and D. Alves, *Estimation of longitudinal bunch characteristics in the LHC using Schottky-based diagnostics*, *Phys. Rev. Accel. Beams* **23** (2020) 062803.

[9] K. Lasocha and D. Alves, *Estimation of transverse bunch characteristics in the LHC using Schottky-based diagnostics*, *Phys. Rev. Accel. Beams* **25** (2022) 062801.

[10] D. Alves and K. Lasocha, *Kalman filter-based longitudinal phase-space reconstruction method for hadron machines*, *Phys. Rev. Accel. Beams* **24** (2021) 072801.

[11] M. Betz, O.R. Jones, T. Lefevre and M. Wendt, *Bunched-beam Schottky monitoring in the LHC*, *Nucl. Instrum. Meth. A* **874** (2017) 113.

[12] J.L. Laclare, *Bunched beam coherent instabilities*, in the proceedings of the *CAS-CERN Accelerator School: Accelerator Physics*, Oxford, U.K., 16–27 September 1985, S. Turner, ed., CERN Yellow Reports: School Proceedings, CERN, Geneva (1987), pp. 264–326 [DOI:10.5170/CERN-1987-003-V-1.264].

[13] H. Wiedemann, *Particle Accelerator Physics*, Springer, Berlin, Germany (2015) [DOI:10.1007/978-3-319-18317-6].

[14] Z. Szabó, *On the analytical methods approximating the time period of the nonlinear physical pendulum*, *Period. Polytech. Mech. Eng.* **48** (2004) 73.

[15] I.S. Gradshteyn and I.M. Ryzhik, *Table of Integrals, Series, and Products*, D. Zwillinger and V. Moll, eds., Elsevier (2007).

[16] G. Stupakov, R. Lindberg and B. Podobedov, *Wakefields and collective beam instabilities*, *U.S. Particle Accelerator School*, Houston, TX, U.S.A. (2023), https://www.slac.stanford.edu/ stupakov/uspas23/2023-01-20/2022-12-07-LECTURES.pdf.

2024 JINST 19 P03017